# CrystEngComm

Accepted Manuscript






ROYAL SOCIETY OF CHEMISTRY

www.rsc.org/crystengcomm

Journal Name

RSCPublishing

ARTICLE

# Mesoporous $V_2O_5$/Ketjin black nanocomposites for all-solid-state symmetric supercapacitors

Cite this: DOI: 10.1039/xoxxoooooox

Tao Peng,[a] Jun Wang,*[,a] Qi Liu,[a] Jingyuan Liu[a] and Peng Wang[b]

Received ooth January 2012,
Accepted ooth January 2012

DOI: 10.1039/xoxxoooooox

www.rsc.org/

$V_2O_5$/Ketjin black (VK) nanocomposites with mesoporous mica-like structure were prepared by a facile sol-gel method. Through a dip-dry process, the VK nanocomposites were successfully assembled on nickel foams with controlable mass loadings. The as-prepared electrode (VK2) shows a high areal capacitance (3.9506 $Fcm^{-2}$ at 5 $mAcm^{-2}$) and good cycling stability (90% after 8000 cycles) in a LiCl/PVA gel electrolyte. Furthermore, the VK nanocomposites-based all-solid-state symmetric supercapacitor can provide the maximum energy density of 56.83 Wh $kg^{-1}$. Such excellent electrochemical performance may promote the VK nanocomposites as a promising electrode material for practical applications.

## 1. Introduction

Electrochemical energy storage (EES) in the form of electrochemical capacitors and batteries is widely used in the light-duty vehicles, portable electronics, metro trains and tramways.[1-2] However, to meet the higher requirements of future systems, we need to improve their performance by design new materials with high energy density and power densitysimultaneously.[3]To address all the technological challenges, most attention has focused on pseudocapacitive materials (such as $RuO_2$, NiO, $MnO_2$, $V_2O_5$) which have the potential of achieving high energy density at high charge /discharge rates, bridging supercapacitors and batteries.[3-5] Moreover, facile and cost-effective methods are still required for scale-up and practical application.[1]

Among many pseudocapacitive materials, $V_2O_5$ is of particular interest due to its ability to intercalate lithium ions, which can facilitate the EES process.[6-7] In comparison to $RuO_2$, $V_2O_5$ is abundant, inexpensive and environmentally friendly.[8-9] More importantly, $V_2O_5$ has rich oxidation states ($V^{5+}$, $V^{4+}$, $V^{3+}$, $V^{2+}$), allowing it achieve high capacitance than other metal oxides.[10] As a result, $V_2O_5$ has been widely studied as electrode materials for pseudocapacitors and batteries.[6-10,32-33] However, its low electronic conductivity and poor cycling stability are heavily limit its industrial application.[7-10]

Various methods have been reported to improve the electronic conductivity of $V_2O_5$.[6-17] For example, Rao and co-workers hybridized carbon nanotube (CNT) with $V_2O_5$, forming high conductive composites.[11] More recently, Lou et al. developed an additive-free solvothermal method to synthesize 3D porous $V_2O_5$ hierarchical microspheres, highly enhancing the electronic conductivity of $V_2O_5$.[6] However, the CNT is expensive and the method for nanostructuring $V_2O_5$ is also uncontrollable. Therefore, a cost-effective and controllable method is urgently needed.

The poor cycling stability of $V_2O_5$ is mainly attributed to the dissolution of electrode material and structural instability during the charge/discharge process.[18] Firstly, $V_2O_5$ can easily forms soluble species in aqueous electrolytes.[19] Secondly, the microstructure of $V_2O_5$ was severely damaged in the lithium ion intercalation/disintercalation process.[20] As a result, numerous efforts also have been paid to addressing this problem.[12,19] For example, LiTFSI, a organic electrolyte, has been used to prevent the dissolution of $V_2O_5$ for supercacitors.[12] However, this organic electrolyte can not solve the structure pulverization problem during lithium ion intercalation /disintercalation process. Therefore, Li and his coworkers developed a LiCl/PVA gel electrolyte which can addresses the dissolution of $V_2O_5$ by minimizing water content and serves as a matrix to maintain the microstructure of $V_2O_5$ at the same times.[19]

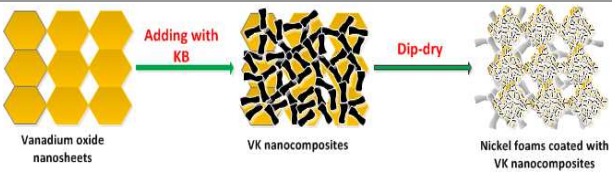


Sch.1 The process of fabricate $V_2O_5$/Ketjin black (KB) nanocomposites electrodes

As a proof-of-concept, we present a facile sol-gel method to produce $V_2O_5$/Ketjin black (KB) nanocomposites electrodes with microstructures and controllable mass loadings (Sch. 1). First, the $V_2O_5$ nanosheets could be easily obtained by a facile sol-gel method. Second, considering that the low electronic conductivity of $V_2O_5$ and the cost-effective and conductive

properties of KB,[21-23] $V_2O_5$/KB (VK) nanocomposites could be achieved by a ultrasonic and stirring process. Third, through the dip-dry process which was reported in our previous work,[24] the VK nanocomposite was successfully assembled on the nickel foams without adding binders. In order to demonstrate the electrochemical performance of the as-prepared electrodes prepared, we fabricated the VK nanocomposites-based symmetrical supercapacitors and investigated their electrochemical performance in a LiCl/PVA gel electrolyte. As a result, the unique electrode shows a competitive areal capacitance (3.95 F $cm^{-2}$ at 5 mA $cm^{-2}$) and high cycling stability (90% capacitance retention after 8000 cycles). The corresponding symmetrical supercapacitor device exhibits energy densities of 56.82 Wh $kg^{-1}$ at a power density of 321 W $kg^{-1}$. Such high performance may promote it for practical application.

## 2. Experimental

### 2.1 Surface modification of KB

All the chemicals were purchased and used directly without further purification. To address the hydrophobic problem of KB, surface modification was performed by a method which was reported in the literature.[25] 10 g KB was added into 1L $HNO_3$ (20 wt%), stirring for 3h at 353K. The resultant product was obtained by filtration, washed with deionized water until the filtrate was neutral, and dried at 353 K for 12h. This modified KB was noted as m-KB.

### 2.2 Preparation of VK nanocomposites

$V_2O_5$ sol was prepared as follow: 1.82 g of $V_2O_5$ power was added to 48 mL deionized water with stirring to form a light yellow solution. Then, 12 mL of 30% $H_2O_2$ was added dropwise to the above solution, stirred for 10 min and subjected to ultrasound for 15 min to form an orange solution.

To synthesize the VK nanocomposites, 0 g, 0.25 g, 0.5 g, 1 g m-KB was dispersed into $V_2O_5$ sol, respectively. After stirring for 10 min, the above mixtures were subjected to ultrasound for 3 h at 298 K.

### 2.3 Interfacial assembly of VK nanocomposites on the nickel foams.

Nickel foams (50×25×1 mm, PPI: 110) were rolled to a thickness of 0.5 mm before use. The treated nickel foams were immersed in a 3 M HCl solution for 15 min to remove the surface oxide layer, and then soaked in a 0.02 M $NiCl_2$ before they were used.

The nickel foam with the surface treatment was dipped into the above slurry solutions and immediately removed. After drying in an oven at 353K for 15 min, the dip-dry process was repeated one time to increase the mass loading on the nickel foam. The nickel foams was rinsed with deionized water and ethanol to remove residual ions. The VK nanocomposites with different $V_2O_5$/KB weight percent ratios were marked as V, VK1, VK2, VK3.

### 2.4 Preparation of LiCl/PVA gel electrolyte and assembly of supercapacitor devices.

The LiCl/PVA gel electrolyte was prepared by a reported method with a little modification.[19] 4 g polyvinyl alcohol (PVA) Power was completely dispersed in 40 mL deionized water at 90 °C with stirring. Then, 8.5 g LiCl was slowly added into the PVA solution under vigorous stirring until a homogeneous solution was formed. The obtained solution was cooled at 298 K.

The all-solid-state supercapacitors with LiCl/PVA gel were fabricated as follow: A piece of filter paper and two pieces of nickel foams (with an overlapped area of 1.0 cm×1.0 cm) coated with VK nanocomposites were immersed into the LiCl/PVA gel electrolyte for 3 min and then dried in air for 30 min. The assembled supercapacitor device was further dried at 40 °C in oven for 24 h to remove the water content. The device was then sealed with insulating epoxy.

### 2.5 Characterization

The crystal phase of the materials were investigated by X-ray diffraction (XRD) (Rigaku TTR-III, Cu Kα, $\lambda$ = 0.15406 nm ). The near-surface elemental composition of the VK product was measured by EDS (JEOL JSM-6480A). Fourier transform infrared (FT-IR) absorption spectra were applied to determine the surface modification result of VK. The $N_2$ sorption measurement were conducted using TriStar II 3020 2.00 instrument at 195.850 °C (77 K). Scanning electron microscopy-energy dispersive spectroscopy (SEM-EDS) (JEOL JSM-6480A) and transmission electron microscopy (TEM) (Philips CM 200 FEG, 200 kV) were performed to measure the morphology of the samples.

### 2.6 Electrochemical measurements

Electrochemical measurement was performed in a two-electrode configuration on a CHI 760D electrochemical workstation. One of the VK electrode serves as the working electrode while the same VK electrode serves as the counter electrode and the reference electrode. The mass loadings of the VK nanocomposites electrodes were 4.02, 4.10, 4.08, 4.13 mg $cm^{-2}$ for V, VK1, VK2, VK3, respectively. The as-prepared LiCl/PVA gel was served as electrolyte.

### 2.7 Calculations

For galvanostatic charge/discharge curves, the areal specific capacitance $C_s$ (F $cm^{-2}$), the gravimetric specific capacitance $C_m$ (F $g^{-1}$), and equivalent series resistance $R_{ESR}$ ($\Omega$) were calculated using the following equations (1)-(3), respectively:

$$C_s = \frac{It}{A\Delta V} \quad (1)$$

$$C_m = \frac{4I}{mdV/dt} \quad (2)$$



 

$$R_{ESR} = \frac{V_{drop}}{2I} \quad (3)$$

where I (A) is the discharge current, t (s) is the discharge time, ΔV (V) is the applied potential region, A ($cm^2$) is the area of the electrode, m (g) is the total mass of the two electrode materials, dV/dt ($V\ s^{-1}$) is the slope obtained by fitting a straight line to the discharge curve and $V_{drop}$ (V) is estimated from the voltage drop at the beginning of the discharge curve.

The energy density E ($Wh\ kg^{-1}$) and the power density P ($w\ kg^{-1}$) of the all-solid-state supercapacitor were calculated by equations (4)-(5), respectively:

$$E = \frac{1}{2} C_{SP} V^2 \quad (4)$$

$$P = \frac{E}{t} \quad (5)$$

where the $C_{SP}$ ($F\ g^{-1}$) is the gravimetric specific capacitance of the supercapacitor, V is the discharge voltage excluding the initial voltage drop.

## 3. Results and discussion

### 3.1 Synthesis of VK nanocomposites and its characterization

As a cost-effective conductive material, KB owns a large specific surface area (~1270 $m^2g^{-1}$) and serves as a conductive bridge to provide more conductive path.[21-23] In comparison to CNT and conductive polymer which have been used in previous work,[11-14, 17, 26] KB is more suitable to hybrid with $V_2O_5$ to form low-cost nanocomposites. However, the hydrophobic property of KB highly hinders the hybrid process.[25] To address this tough problem, surface modification treatment was performed by adding the carboxylic moiety (-COOH) to KB. As shown on Fig. 1, the FT-IR spectra of KB and m-KB confirm the surface modification process. The new bonds at 3423 and 1720 $cm^{-1}$ could be attributed to the stretching vibrations of the –OH and C=O, respectively. It indicates the existence of the carboxylic moiety (-COOH), which is not seen in original KB (Fig.1). Therefore, the successful surface modification treatment of KB could facilitate m-KB penetrate into $V_2O_5$ sol.

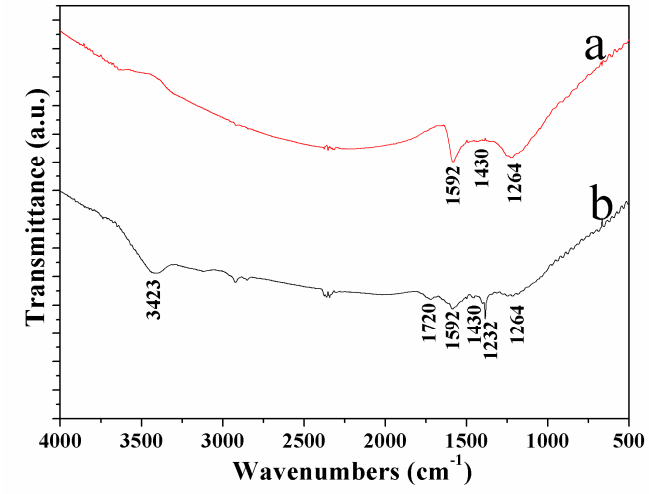


Fig. 1 FT-IR spectra of KB (a) and m-KB (b).

After adding m-KB to $V_2O_5$ sol, the VK nanocomposites were obtained by an ultrasonic and stirring process with dried at 353K. XRD patterns in Fig. 2 confirm the formation of VK nanocomposites. As shown on Fig. 2 a, the XRD pattern indicates a series of (00l) peeks which are consistent with layer structured hydrous $V_2O_5$.[25, 27] The peaks located at 2θ values of 8.1°, 22.5°, 27.1°, 38.8° correspond to the (001), (003), (004), (005) diffraction planes of hydrous $V_2O_5$.[27] No other clear peak was observed showing the poor crystallization of the as-prepared $V_2O_5$.[23] The missing (002) peak reveals the formation of double $V_2O_5$ nanosheets in each layer.[25] In Fig. 2c-d, it indicates three diffraction peaks at 8.1°, 27.1°, 38.8°, respectively, which could be indexed to the characteristic peaks of the hydrous $V_2O_5$. What's more, the only characteristic peak of m-KB could be found in VK1, VK2 and VK3. According to the above XRD analysis, it demonstrates that m-KB is introduced into $V_2O_5$ matrix successfully. EDS patterns of the as-prepared material also confirm the existence of VK (Fig.S1). The element ratio of V, O, C is 1: 2.62:2.08, matching well with the formula of $V_2O_5$ and the V/C element ratio of VK2.

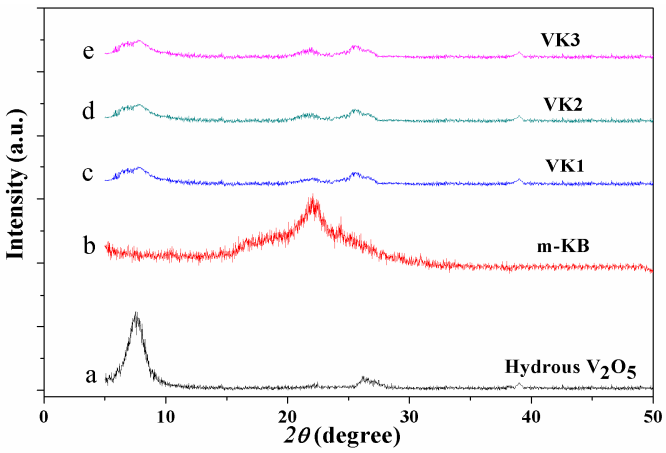


Fig. 2 XRD patterns of hydrous $V_2O_5$ (a), m-KB (b), VK1 (c), VK2 (d) and VK3 (e).

The TEM images (Fig.3a-c) confirm the nanosheet structure of the as-prepared VK nanocomposites. The bulk $V_2O_5$ was transformed to $V_2O_5$ nanosheets via a sol-gel method and a subsequent ultrasound treatment. (Fig. 3 a) As can be seen from Fig. 3a-c, m-KB was uniformly dispersed within the $V_2O_5$ nanosheets, forming a continuous conductive network. The m-KB was closely contacted with $V_2O_5$ nanosheet, which enhanced the electronic conductivity of $V_2O_5$. It is worth to

noting that the carboxylic moiety (-COOH) on KB surface might combine with $V_2O_5$ to form chemical bonds, ensuring more tight contacts between $V_2O_5$ and KB.[23, 28] When the TEM images of Fig. 3 d magnified, it could be clearly observed that the mesopores with the estimated size of 5-8 nm are uniformly distributed in the surface of the VK nanocomposites. The Brunauer-Emmett-Teller (BET) surface area of the obtained VK nanocomposites are calculated to be 22.07, 74.84, 264.72 $m^2g^{-1}$ for VK1, VK2, VK3, correspondingly (Tab.S1 and Fig. S2a). Comparing to the pristine $V_2O_5$, the surface area of VK nanocomposites were highly enhanced due to the introduction of m-KB. The mesoporous feature of VK2 nanocomposites can further confirmed by the pore-size distribution analysis (Fig.S2b), indicating that a pore size arrange of 6-7 nm which is also consistent with the TEM analysis.

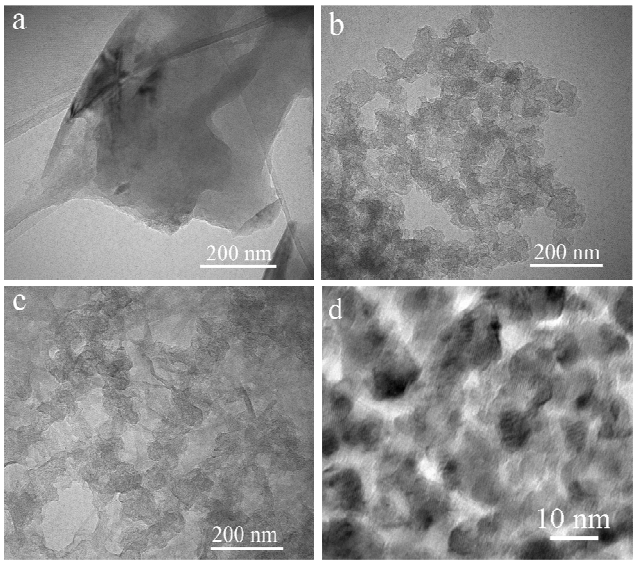

Fig.3 TEM images of V (a), m-KB (b), VK(c)(d) .

### 3.2 Interfacial assembly of VK nanocomposites on the nickel foams

Interfacial assembly of VK nanocomposites on the nickel foams was performed by a facile dip-dry process. From Fig. 4a and c, it is clearly observed that VK nanocomposites may be more suitable for interfacial assembly than $V_2O_5$ nanosheets. For VK nanocomposites, the aggregated films tightly coat the skeletons of nickel foams and cover the pores which may lead to high mass loadings on the nickel foams. However, the $V_2O_5$ nanosheets were loosely attached with the substrate, resulting the mass loss during the dipping number increased. When the SEM images magnified, it could be see that the $V_2O_5$ thin film with a smooth surface were indeed uniform (Fig. 4b). With respect to Fig. 4d, it is interesting to observe that the mica-like building blocks were formed by the stack of VK nanocomposites. This mica-like structure of VK thin films could provide an accessible surface area and more active sites, resulting in an obviously increased capacitance.[29]

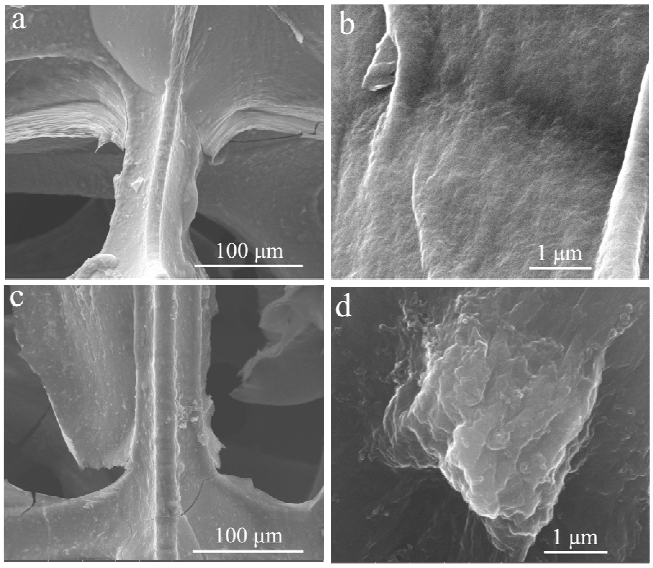

Fig. 4 SEM image of V (a) (b) and VK (c) (d) on nickel foams.

The mass loadings of VK nanocomposites on nickel foams could be well-controlled by the dip-dry process. As the dipping number increased, the VK nanocomposites gradually covered on nickel foams, leading the uniformly increase of mass loading. (Fig. 5) Therefore, the dip-dry process exhibits its high controllability. What's more, the low volatility implies the experimental results could be easily repeated which is important for industry application.[30]

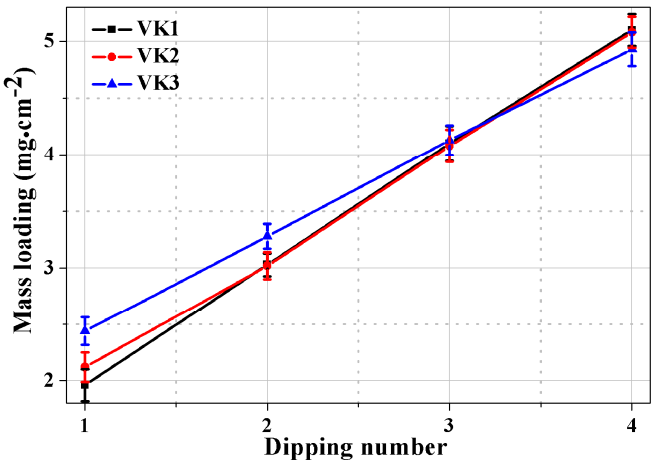

Fig. 5 Mass loading of VK on nickel foams.

### 3.3 Electrochemical measurement

In order to explore electrochemical performance of the VK-based supercapacitors, cyclic voltammetry (CV), galvanostatic charge/discharge measurements were performed in a LiCl/PVA

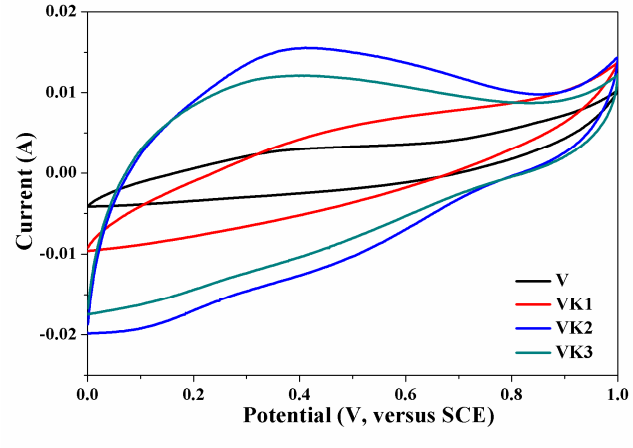


Fig. 6 CV spectra for the V, VK1, VK2, VK3 at 5 $mVs^{-1}$, respectively.

gel electrolyte using a two-electrode system at room temperature. Fig. 6 demonstrates the CV spectra of V, VK1, VK2, VK3 at the scan rate of 5 $mVs^{-1}$ in a potential range of 0 to 1.0 V. Clearly, the shapes of the CV curves are distinctly different from the CV curves obtained in three-electrode system.[8-11, 13-17]The relatively apparent redox peaks in the CV curves could be ascribed to typical pseudocapacitive performance of $V_2O_5$ nanosheets. The integrated CV area for the VK nanocomposites/nickel foams electrodes (VK1, VK2, VK3) are obviously larger than the $V_2O_5$ nanosheets/nickel foams electrode (V), confirming that the VK nanocomposites material is more suitable for supercapacitors. Furthermore, the VK2 electrode shows higher capacitance than its corresponding VK1 and VK3 electrode. It may cause by their different $V_2O_5$/KB mass ratio. The $V_2O_5$/KB mass ratio of VK2 may benefit to keeping the balance between conductivity and capacity.

Galvanostatic charge/discharge measurements were conducted in LiCl/PVA gel electrolyte at current density of 5 to 40 $mAcm^{-2}$. As shown on Fig. 7a, the nonlinear charge/discharge curves reveal the main contribution of pseudocapacitance from $V_2O_5$, in agreement with the above CV analysis result. What's more, the charge/discharge curves are highly symmetrical, indicating the excellent electrochemical reversibility of the as-prepared electrodes.[19] In comparison to V electrode, the VK electrodes own wider potential window and larger capacitance. At the same current density of 5 $mAcm^{-2}$, the areal capacitances $C_s$ are about 0.1441, 1.4189, 3.9506 and 2.0334 $Fcm^{-2}$ for V, VK1, VK2, VK3, respectively (Fig. 7b). This enhanced capacitance of VK electrodes could be attributed to the high electrical conductivity of KB. The VK1, VK2 and VK3 electrodes retain 40%, 45% and 44% of their initial capacitances, when the current density increased from 5 to 40 $mAcm^{-2}$. The relative low rate performance could be ascribed to slower ion diffusion in gel electrolyte.[19] The gravimetric specific capacitance $C_m$ was also be calculated according to equation (2). From Fig. S3, the VK2 electrode achieves a maxi

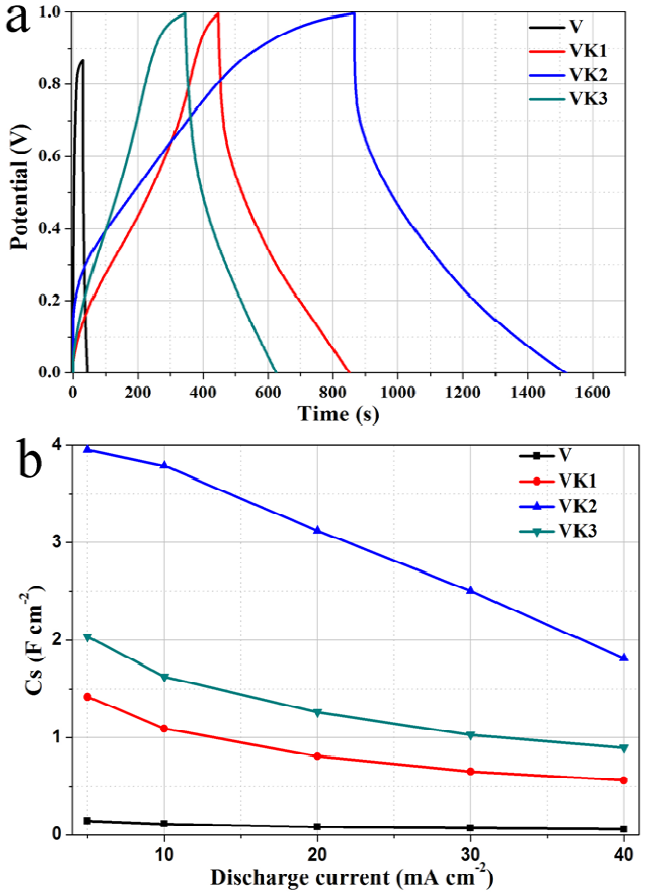


Fig.7 (a) Charge and discharge curves for the V, VK1, VK2, VK3 at current density of 5 mA $cm^{-2}$ , respectively; ( b) area capacitance ($C_s$) for the V, VK1, VK2, VK3, respectively.

-mum gravimetric specific capacitance of 1633.99 $Fg^{-1}$ at 5 $mAcm^{-2}$. Such high specific capacitance is competitive in compare with previous works.[8-11, 13-17] All the results prove that VK electrodes exhibit better electrochemical capacitive performance than the counter V electrode.

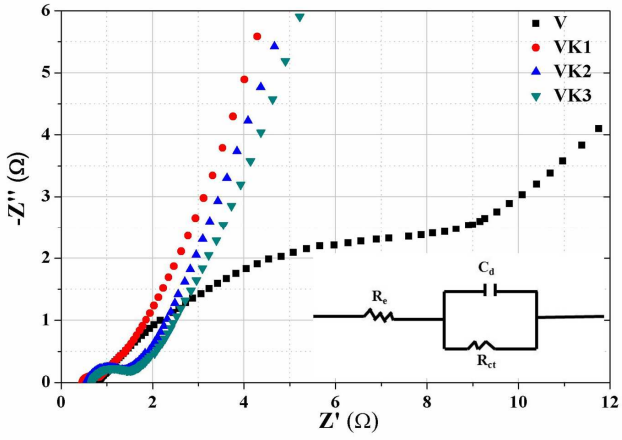


Fig.8 EIS spectra for the V, VK1, VK2, VK3 at open circuit voltage, respectively.

To verify our hypothesis that the KB could highly increase the electric conductivity of $V_2O_5$, the V, VK1, VK2, VK3 electrodes are selected to be measured by electrochemical impedance spectroscopy (EIS). As seen in Fig. 8 and Tab.S3, the VK1, VK2, VK3 electrodes show nearly vertical lines in the low frequency region, revealing their more ideal capacitive property than the V electrode.[31] Besides, the charge-transfer and ion diffusion resistance ($R_{ct}$) of the VK1, VK2, VK3 electrodes which could be calculated from the diameters of the semicircles are smaller than the V electrode.[31] All EIS results prove that the electric conductivity of $V_2O_5$ was highly improved via the introduction of KB, which is also consistent with the ESR data obtained by galvanostatic charge/discharge measurements (Fig. S4).

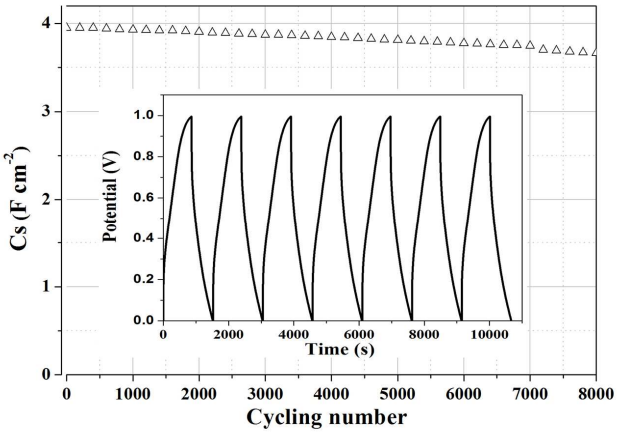


Fig. 9 Cycling performance of the VK2 for 8000 cycles at 5 $mAcm^{-2}$.

The cycling stability performance of VK electrode (VK2) was investigated at current density of 5 $mAcm^{-2}$ for 8000 cycles. As seen in Fig. 9, the areal capacitance of the VK2 electrode was nearly unchanged during the repeated charge/discharge process. After 1000 cycles, the areal capacitance gradually decreased with the increase of cycle number, and 90% of the initial areal capacitance retained after 8000 cycles. The high cycling stability performance of VK electrode can be assigned to the LiCl/PVA gel electrolyte which used in electrochemical measurement. The LiCl/PVA gel serves as a matrix to maintain the microstructure of VK during the repeated charge/discharge process.[19]

In order to measure the device performance of the all-solid-state symmetric supercapacitors based on VK nanocomposites, the energy density (E) and the power density (P) were be calculated by equation (4) and (5). According to the Ragone plot in Fig. 10 and Tab. S4, the as-fabricated supercapacitor based on VK2 shows greatly superior electrochemical performance in compare with the VK1-based and VK3-based supercapacitors. The maximum energy density of 56.83 $Whkg^{-1}$ (303 $Wkg^{-1}$) and power density 2423 $Wkg^{-1}$ (30.86 $Whkg^{-1}$) were obtained at the potential window of 1.0 V, indicating its ability to provide high energy density with little sacrifice in power density. The maximum energy density of the VK2-based supercapacitor is comparable to previous $V_2O_5$-based supercapacitor reported.[12-14, 32-33]

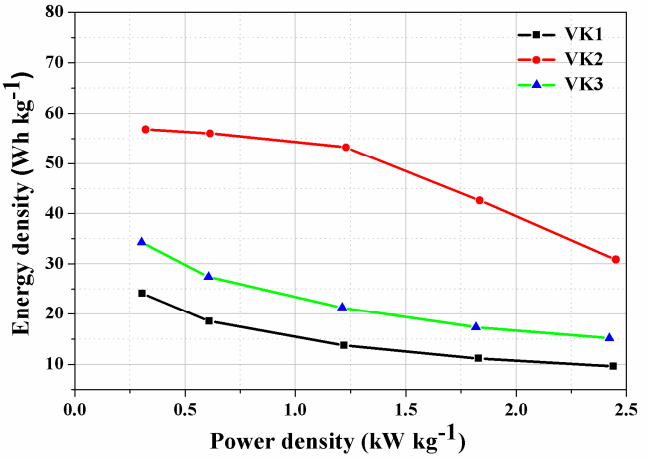


Fig.10 Ragone plot of the VK nanocomposites all-solid-state supercapacitor device measured by LiCl/PVA gel electrolyte.

The enhanced electrochemical performances of VK nanocomposites could be attributed to the following aspects. Firstly, the mica-like structure of VK thin films highly favors ions contact with electroactive sites, which effectively facilitate the pseudocapacitive effect of the supercacitor.[29] Secondly, KB greatly enhanced the electric conductivity of VK nanocomposites, significantly facilitating redox reactions near the surface of electrodes.[34-35] Finally, LiCl/PVA gel electrolyte maintains the microstructure of VK during the repeated charge/discharge process, thus resulting in high cycling performance.[19]

## 4. Conclusions

In summary, the $V_2O_5$/Ketjin black nanocomposites with mesoporous mica-like structure were prepared by a facile sol-gel method. Through a dip-dry process, the $V_2O_5$/Ketjin black nanocomposites were successfully assembled on nickel foams with controlable mass loadings. Owing to the mesoporous mica-like structure and high electric conductivity, the as-prepared electrode (VK2) indicates an competitive electrochemical performance in a LiCl/PVA gel electrolyte. It shows a high areal capacitance (3.9506 $Fcm^{-2}$ at 5 $mAcm^{-2}$) and good cycling stability (90% after 8000 cycles). Furthermore, the VK-based all-solid-state symmetric supecapacitor can provide the maximum energy density of 56.83 Wh $kg^{-1}$. Such high electrochemical performance may promote the $V_2O_5$/Ketjin black nanocomposites as a promising electrode material for practical applications.

## Acknowledgements

This work was supported by National Natural Science Foundation of China (21353003), Special Innovation Talents of

Harbin Science and Technology (2013RFQXJ145), Fundamental Research Funds of the Central University (HEUCFZ), Key Program of the Natural Science Foundation of Heilongjiang Province (ZD201219), Program of International S&T Cooperation special project (2013DFA50480).

## Notes

[a] Key Laboratory of Superlight Material and Surface Technology, Ministry of Education, Harbin Engineering University, 150001, PR China.
[b] State Key Laboratory of Polymer Physics and Chemistry, Changchun Institute of Applied Chemistry, Chinese Academy of Sciences, 130022, PR China.
* Corresponding author: Tel.: +86 451 8253 3026;
Fax: +86 451 8253 3026;
E-mail: junwang@hrbeu.edu.cn

Electronic Supplementary Information (ESI) available: [details of any supplementary information available should be included here]. See DOI: 10.1039/b000000x/

## References

1. J. R. Miller and P. Simon, *Science*, 2008, **321**, 651-652.
2. P. Simon and Y. Gogotsi, *Nat. Mater.*, 2008, **7**, 845-854.
3. V. Augustyn, P. Simon and B. Dunn, *Energ. Environ. Sci.*, 2014, **7**, 1597-1614.
4. B. E. Conway, V. Birss and J. Wojtowicz, *J. Power Sources*, 1997, **66**, 1-14.
5. P. Simon, Y. Gogotsi and B. Dunn, *Science*, 2014, **343**, 1210-1211.
6. C. F. Zhang, Z. X. Chen, Z. P. Guo and X. W. Lou, *Energ. Environ. Sci.*, 2013, **6**, 974-978.
7. X. W. Zhou, G. M. Wu, J. D. Wu, H. Y. Yang, J. C. Wang and G. H. Gao, *Phys. Chem. Chem. Phys.*, 2014, **16**, 3973-3982.
8. B. Saravanakumar, K. K. Purushothaman and G. Muralidharan, *ACS Appl. Mater. Interfaces*, 2012, **4**, 4484-4490.
9. J. Shao, X. Y. Li, Q. T. Qu and H. H. Zheng, *J. Power Sources*, 2012, **219**, 253-257.
10. J. X. Zhu, L. J. Cao, Y. S. Wu, Y. J. Gong, Z. Liu, H. E. Hoster, Y. H. Zhang, S. T. Zhang, S. B. Yang, Q. Y. Yan, P. M. Ajayan and R. Vajtai, *Nano Lett.*, 2013, **13**, 5408-5413.
11. M. Jayalakshmi, M. M. Rao, N. Venugopal and K. B. Kim, *J. Power Sources*, 2007, **166**, 578-583.
12. S. D. Perera, B. Patel, N. Nijem, K. Roodenko, O. Seitz, J. P. Ferraris, Y. J. Chabal and K. J. Balkus, *Adv. Energy Mater.,* 2011, **1**, 936-945.
13. I. Shakir, J. H. Choi, M. Shahid, S. A. Shahid, U. A. Rana, M. Sarfraz and D. J. Kang, *Electrochim. Acta*, 2013, **111**, 400-404.
14. I. Shakir, Z. Ali, J. Bae, J. Park and D. J. Kang, *Nanoscale*, 2014, **6**, 4125-4130.
15. B. H. Kim, C. H. Kim, K. S. Yang, A. Rahy and D. J. Yang, *Electrochim. Acta*, 2012, **83**, 335-340.
16. B. H. Kim, K. S. Yang and D. J. Yang, *Electrochim. Acta*, 2013, **109**, 859-865.
17. I. H. Kim, J. H. Kim, B. W. Cho, Y. H. Lee and K. B. Kim, *J. Electrochem. Soc.*, 2006, **153**, 989-996.
18. Y. Liu, M. Clark, Q. Zhang, D. Yu, D. Liu, J. Liu and G. Cao, *Adv. Energy Mater.*, 2011, **1**, 194-202.
19. G. M. Wang, X. H. Lu, Y. C. Ling, T. Zhai, H. Y. Wang, Y. X. Tong and Y. Li, *ACS Nano*, 2012, **6**, 10296-10302.
20. D. W. Liu, Y. Y. Liu, S. L. Candelaria, G. Z. Cao, J. Liu and Y. H. Jeong, *J. Vac. Sci. Technol. A*, 2012, **30**.
21. X. Yang, Y. L. Xu, H. Zhang, Y. A. Huang, Q. Jiang and C. J. Zhao, *Electrochim. Acta*, 2013, **114**, 259-264.
22. P. Agbo, J. R. Heath and H. B. Gray, *J. Phys. Chem. B*, 2013, **117**, 527-534.
23. D. S. Kim and Y. J. Park, *Electrochim. Acta*, 2014, **132**, 297-306.
24. Z. Y. Qian, T. Peng, L. T. Qu, J. Wang and P. Wang, *J. Mater. Chem. A*, 2014, **2**, 4894-4898.
25. L. Yu, C. X. Zhao, X. Long and W. Chen, *Micropor. Mesopor. Mater.*, 2009, **126**, 58-64.
26. J. Yang, T. B. Lan, J. D. Liu, Y. F. Song and M. D. Wei, *Electrochim. Acta*, 2013, **105**, 489-495.
27. J. Xu, H. J. Sun, Z. L. Li, S. Lu, X. Y. Zhang, S. S. Jiang, Q. Y. Zhu and G. S. Zakharova, *Solid State Ion.*, 2014, **262**, 234-237.
28. S. L. Chen, H. B. Wu, H. C. Hu, Y. H. Mo, J. L. Yin, G. L. Wang, D. X. Cao, Y. M. Zhang, B. F. Yang and P. L. She, *Solid State Ion.*, 2013, **233**, 1-6.
29. D. M. Yu, Y. J. Qiao, X. Y. Zhou, J. Wang, C. Li, C. G. Chen and Q. S. Huo, *J. Power Sources*, 2014, **266**, 1-6.
30. T. Peng, Z. Qian, J. Wang, D. Song, J. Liu, Q. Liu and P. Wang, *J. Mater. Chem. A*, 2014, **2**, 19376-19382.
31. M. K. Liu, W. W. Tjiu, J. S. Pan, C. Zhang, W. Gao and T. X. Liu, *Nanoscale*, 2014, **6**, 4233-4242.
32. L.M. Chen, Q.Y. Lai, Y.J. Hao, Y. Zhao and X.Y. Ji, *J. Alloy. Compd.*, 2009, **467**, 465-471.
33. Q. T. Qu, Y. Shi, L. L. Li, W. L. Guo, Y. P. Wu, H. P. Zhang, S. Y. Guan and R. Holze, *Electrochem. Commun.*, 2009, **11**, 1325-1328.
34. G. Q. Zhang and X. W. Lou, *Adv. Mater.*, 2013, **25**, 976-979.
35. J. Jiang, Y. Y. Li, J. P. Liu, X. T. Huang, C. Z. Yuan and X. W. Lou, *Adv. Mater.*, 2012, **24**, 5166-5180.

# Graphic abstract

# A facile method to fabricate mesoporous $V_2O_5$/ Ketjin black nanocomposites and their all-solid-state symmetric supercapacitor

Tao Peng,[a] Jun Wang*,[a] and Peng Wang[b]

[a] Key Laboratory of Superlight Material and Surface Technology, Ministry of Education, Harbin Engineering University, 150001, PR China.

[b] State Key Laboratory of Polymer Physics and Chemistry, Changchun Institute of Applied Chemistry, Chinese Academy of Sciences, 130022, PR China.

* Corresponding author: Tel.: +86 451 8253 3026; fax: +86 451 8253 3026; E-mail: junwang@hrbeu.edu.cn.

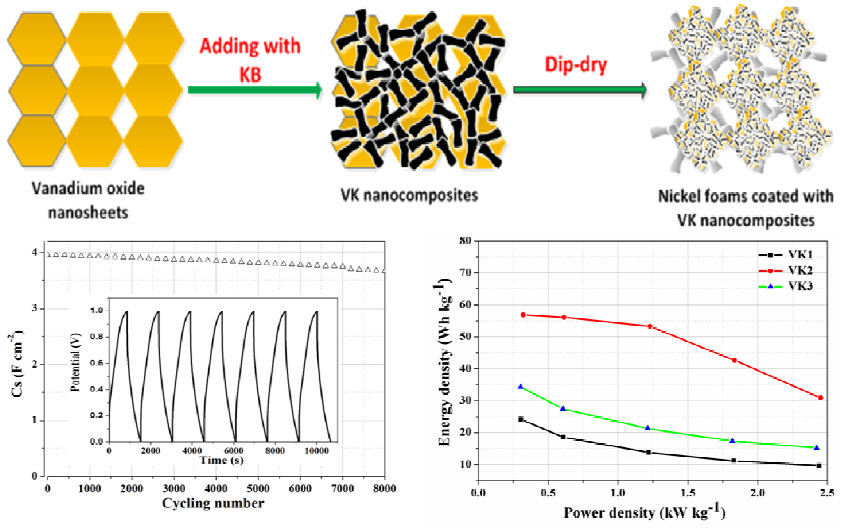


$V_2O_5$/Ketjin black (VK) nanocomposites with mesoporous mica-like structure were prepared by a facile sol-gel method. The as-prepared electrode (VK2) shows a high areal capacitance (3.9506 $Fcm^{-2}$ at 5 $mAcm^{-2}$) and good cycling stability (90% after 8000 cycles) in a LiCl/PVA gel electrolyte. Furthermore, the VK nanocomposites-based all-solid-state symmetric supercapacitor can provide the maximum energy density of 56.83 Wh $kg^{-1}$, indicating their potential for practical applications.